Surfaces and Interfaces 28 (2022) 101678

Contents lists available at ScienceDirect

Surfaces and Interfaces

journal homepage: www.sciencedirect.com/journal/surfaces-and-interfaces

Hyaluronic acid bisphosphonates as antifouling antimicrobial coatings for PEO-modified titanium implants

Lyudmila V. Parfenova [a,d,*], Zulfia R. Galimshina [a,d], Guzel U. Gil'fanova [a], Eliza I. Alibaeva [a], Ksenia V. Danilko [b,d], Tatyana M. Pashkova [c,d], Olga L. Kartashova [c], Ruzil G. Farrakhov [d], Veta R. Mukaeva [d], Evgeny V. Parfenov [d], Rameshbabu Nagumothu [e], Ruslan Z. Valiev [d]

[a] Institute of Petrochemistry and Catalysis of Russian Academy of Sciences, 141, Prospekt Oktyabrya, Ufa 450075, Russian Federation
[b] Bashkir State Medical University, 3 Lenin Street, Ufa 450000, Russian Federation
[c] Institute of Cellular and Intracellular Symbiosis, Ural Branch of the Russian Academy of Sciences, 11 Pionerskaya, Orenburg 460000, Russian Federation
[d] Ufa State Aviation Technical University, 12 Karl Marx Street, Ufa 450008, Russian Federation
[e] Department of Metallurgical and Materials Engineering, National Institute of Technology, NIT Quarters, Tiruchirappalli 620015, India

ARTICLE INFO

Keywords:
Hyaluronic acid
Bisphosphonates
Michael reaction
Titanium implants
Nanostructured titanium
Plasma electrolytic oxidation
Antimicrobial coating

ABSTRACT

The work is aimed at the development of biocompatible coatings based on bisphosphonic acid derivatives of a natural polymer matrix – hyaluronic acid, for modification of the surface of nanostructured and coarse-grained Ti Grade 4 with a sublayer obtained by plasma electrolytic oxidation (PEO). The synthesis of hyaluronic acid (HA) derivatives was carried out by oxidation of HA with $TEMPO^{+}Cl^{-}$, as well as by the Michael addition of maleimides of γ-aminobutanoic and ε-aminocaproic acid bisphosphonates to SH-functionalized HA. Organic molecules were deposited to the PEO-modified titanium surface by physicochemical adsorption from solutions. The presence of the organic coating in the pores of the PEO-sublayer was confirmed by X-ray photoelectron spectroscopy (XPS). The contact angle measurements showed the increase in the hydrophilicity of the Ti-PEO surface modified with the hyaluronic acid bisphosphonates. The study of biological activity *in vitro* revealed that the HA bisphosphonates are non-toxic, and the coatings based on them decrease the viability of fibroblasts (by 20–40%), osteoblast-like cells MG-63 (by 30–60%), and mesenchymal stem cells (more than 60%) compared to Ti-PEO control surfaces. As a result of antibacterial property studies, a significant decrease in the adhesion of pathogens P. aeruginosa, S. aureus, and E. faecium on the surface of nanostructured titanium modified with PEO and HA derivatives was found. Therefore, the resulting hybrid PEO-organic coatings can contribute to further development of antifouling antimicrobial coatings for metal implants.

1. Introduction

Currently, titanium (Ti) continues to be one of the most demanded metals in implantology. Ti alloys are widely used for orthopedic implants because they exhibit biocompatibility, chemical stability, and excellent mechanical strength [1–3]. For implants, the most significant improvements relate to miniaturization, increased strength, bioactivity, and antibacterial properties; all these provide accelerated osseointegration and facilitate patient rehabilitation [4]. Therefore, the most advanced research in the field of biomaterials includes the design of a new generation of implants based on a biomimetic approach that imitates the living bone at all levels: mechanical, physical, chemical, and biological [5]. It was shown earlier that the formation of a nanostructure in pure titanium leads to increased strength and fatigue life, which removes the limitations of its use for the manufacture of modern implants [6,7]. Along with mechanical properties, changing titanium grain size affects its biological properties [8–10]. For example, the cell cycle, chromatin modification, telomere maintenance, and RNA metabolism are activated on nanostructured titanium [11]. The surface properties of titanium implants are also one of the important key components that ensure the long-term clinical success of the implantation of titanium devices into bone tissue [12–15]. Therefore, methods that change the architecture and composition of the surface layer to meet the properties of the bone tissue and cell membranes are widely developed.

Promising methods for the inorganic layer formation on the titanium surface include anodizing technologies, among which plasma-

* Corresponding author at: Institute of Petrochemistry and Catalysis of Russian Academy of Sciences, 141, Prospekt Oktyabrya, Ufa 450075, Russian Federation.
E-mail address: luda_parfenova@ipc-ras.ru (L.V. Parfenova).

https://doi.org/10.1016/j.surfin.2021.101678
Received 12 August 2021; Received in revised form 9 December 2021; Accepted 11 December 2021
Available online 20 December 2021

electrolytic oxidation stands out because it provides a conversion oxide layer on the metal surface with a high degree of adhesion [16–18]. The PEO mechanism is based on the action of microdischarges that repeatedly pierce and remelt the titanium oxide surface layer (rutile and anatase). This approach helps to obtain coatings with controlled porosity and microstructure similar to the human bone; moreover, a developed network of pores forms a fractal structure with the pores enlarging towards the surface. This morphology provides a smooth change in the elasticity modulus from the metal implant to the bone, which also improves mechanical compatibility. The results of the study of biological activity *in vivo* showed, that PEO coating promotes bone formation and shows a higher level of bone maturation [15,19].

The bioactivity of the inorganic coatings can be significantly improved and adjusted by using an organic matrix, which can mask the implant and/or contain functional fragments that actively interact with various types of cells [20–22]. The surface can be functionalized to prevent the formation of a non-specific protein layer, making the device "invisible" for the cells (so-called antifouling coatings), and, thereby, inhibiting the inflammatory foreign body response. Another complication that prevents osseointegration is a bacterial infection. Bacteria belonging to the so-called ESKAPE panel (E. faecium, S. aureus, K. pneumoniae, A. baumannii, P. aeruginosa, and Enterobacter species) are becoming more common and resistant to traditional antibiotics, and therefore represent a particularly dangerous group of microorganisms [23]. In addition, microorganisms can form antibiotic-resistant biofilms that protect them from environmental stress, inhibit phagocytosis and, thus, impart colonization and long-term existence on the surface of the implant and surrounding tissues [24,25]. Treating such infections is usually very difficult because the bacteria in the biofilm are largely less susceptible to the host's immune system and are well protected from the ingress of antibiotics [26]. One solution consists of the incorporation of antimicrobial agents in the coating and realization of the protection through the gradual release of these agents or contact killing of bacteria. Another way is the development and application of antifouling coatings that reduce bacterial adhesion and biofilm formation [27].

To provide such properties to the surface, polysaccharides, self-assembled monolayers, polyethylene glycols, polyacrylates, etc. are used [20,22]. The coatings based on polysaccharides, in particular glycosaminoglycans (GAGs), have great potential for development, since they possess low toxicity and show high anti-inflammatory properties [28]. Among GAGs, hyaluronic acid (HA) stands out due to its unique biological properties and commercial availability [29–32]. Through interactions with various receptors such as CD44 and TSG-6, HA is a key regulator of inflammation [33,34]. Modification by carboxyl, hydroxyl, or acetamide groups allows the modeling of the physicochemical and biological properties of HA [35]. For example, the C6 oxidation of the N-acetyl-D-glucosamine unit of HA to N-acetyl-D-glucosaminuronic acid gives polyuronic acid – carboxy-HA that exhibits high resistance to the action of testicular hyaluronidase, which is important in the development of drugs with prolonged action with better water solubility than the original HA [36]. The use of HA in organic layers on titanium provides various biological effects *in vitro* and *in vivo* [37–51]; this makes HA a promising candidate for the development of biocompatible coatings for metal implants.

The degree of adhesion of organic molecules to the metal oxide surface, as well as the adsorption of calcium ions on the surface, can be increased by introducing phosphonate groups [52–56]. Polysaccharide phosphorylation [57] is considered as a promising strategy for the design of materials for bone tissue regeneration and cancer therapy [58–61], as well as for application as biologically active coatings on inorganic materials [62,63].

Recently, we developed an approach [64–66], in which the bioactive coating on Ti is formed by a combination of the inorganic porous oxide sublayer, obtained by plasma electrolytic oxidation of titanium surface, and integrin-active RGD-oligopeptide with bisphosphonate anchors, ensuring the reliable attachment of organic molecules to the highly developed oxide surface. As a result of the introduction of such molecules, a significant increase in the viability of fibroblasts and osteoblast-like cells on the PEO-modified metal surface was observed.

The current research aims to design new biocompatible coatings based on the modification of the PEO sublayer with bisphosphonic derivatives of the natural polymer matrix – hyaluronic acid, which high affinity to the metal oxide surface and bioactivity should result in antifouling and antimicrobial properties. The research provides information on the composition, physicochemical properties, and biological activity of the composite coating, consisting of the hybrid organic molecules and inorganic PEO sublayer, and dependence of these properties on the substrate material – nanostructured (nano-Ti) and coarse-grained titanium (CG-Ti).

2. Experimental

2.1. Metal sample preparation and PEO coating

Titanium Grade 4 (ASTM F67) was used as a substrate material. The chemical composition of the Ti Grade 4 is (wt%): Fe - 0.15, C - 0.05, O - 0.36, N - 0.007; H - 0.002, Ti - balance. The nanostructuring of titanium (nano-Ti) was carried out via severe plastic deformation [67] using equal channel angular pressing (ECAP-C) with consequent drawing [68]. As a result, titanium rods with a diameter of 8 mm were obtained. Next, 0.5 mm thick discs were cut out of the rod. The coarse-grained (CG-Ti) samples were cut out from the as supplied rods of the same diameter.

Before the PEO processing, the samples were ground on SiC abrasive paper with 600, 1000, 2000 grit sizes to obtain the roughness value of $Ra < 0.15$ μm. Then the samples were washed in distilled water, cleaned in isopropyl alcohol using an ultrasonic bath for 5 min and dried in air at room temperature. The plasma electrolytic oxidation was carried out using automated equipment with a peak power of 50 kW in the pulsed bipolar regime under voltage control [64–66]. The parameters of the PEO process were maintained at a given level with ±2% accuracy. The PEO process was carried out in a 10-liter glass vessel, equipped with a stainless steel heat exchanger. The electrolyte volume was 5 liters. The PEO processing details are presented in Table 1. Grade 2 titanium alloy wire with a diameter of 1 mm was used as the sample holder. The sample was attached to a loop 8 mm in diameter at the end of the holder.

2.2. Synthesis of conjugates of hyaluronic acid with amino acid bisphosphonates

General Information. The following reagents were used for the synthesis: the low molecular weight (LMW) HA (>0.1 MDa, Germany) were supplied from Leko Style (St.-Petersburg), methanesulfonic acid (98%, Acros Organics), PCl_3 (98%, Acros Organics), γ-aminobutanoic (99+%, Acros Organics) and ε-aminocaproic acid (98.5%, Merk), maleic anhydride (98+%, Acros Organics), N-hydroxysuccinimide (98+%, Acros Organics), dicyclohexylcarbodiimide (DCC, 99%, Acros Organics), Cleland's Reagent (DTT, 98%, ABCR), 4-aminobutyric acid (99+% Acros Organics). Carboxy-HA (2) was prepared by the oxidation of LMW HA with 2,2,6,6-tetramethylpiperidine-1-oxoammonium chloride ($TEMPO^+Cl^-$) [69] (Scheme 1). 4,4′-dithiodibutyric acid dihydrazide (3) was obtained by the method [70], SH-derivative HA (5) was obtained according to the known procedure [71]. The N- maleimidosuccinimide linkers (BMPS, EMCS, and SMCC) were synthesized according to Refs. [72,73]. Maleimide derivatives of γ-aminobutyric and ε-aminocaproic acid bisphosphonates 6–9 were synthesized according to [65].

Spectroscopic studies were carried out by the means of ^1H and ^{31}P NMR on a Bruker AVANCE-500 spectrometer (operating frequency 500.17 MHz (^1H) and 202.48 MHz (^{31}P)). D_2O and $CDCl_3$ were used as the internal standards and solvents. Chemical shifts NMR ^{31}P are given relative to the standard - 85% solution of H_3PO_4 in H_2O (δ_P 0 ppm).

Table 1
PEO processing mode.

Electrolytecomposition	Positive pulse		Negative pulse		Frequency (Hz)	Temperature (°C)	Duration (min.)
	Voltage (V)	Dutycycle (%)	Voltage (V)	Dutycycle (%)			
20 g/l $Na_3PO_4{\cdot}12$ H_2O	470	51	40	26	300	20	5

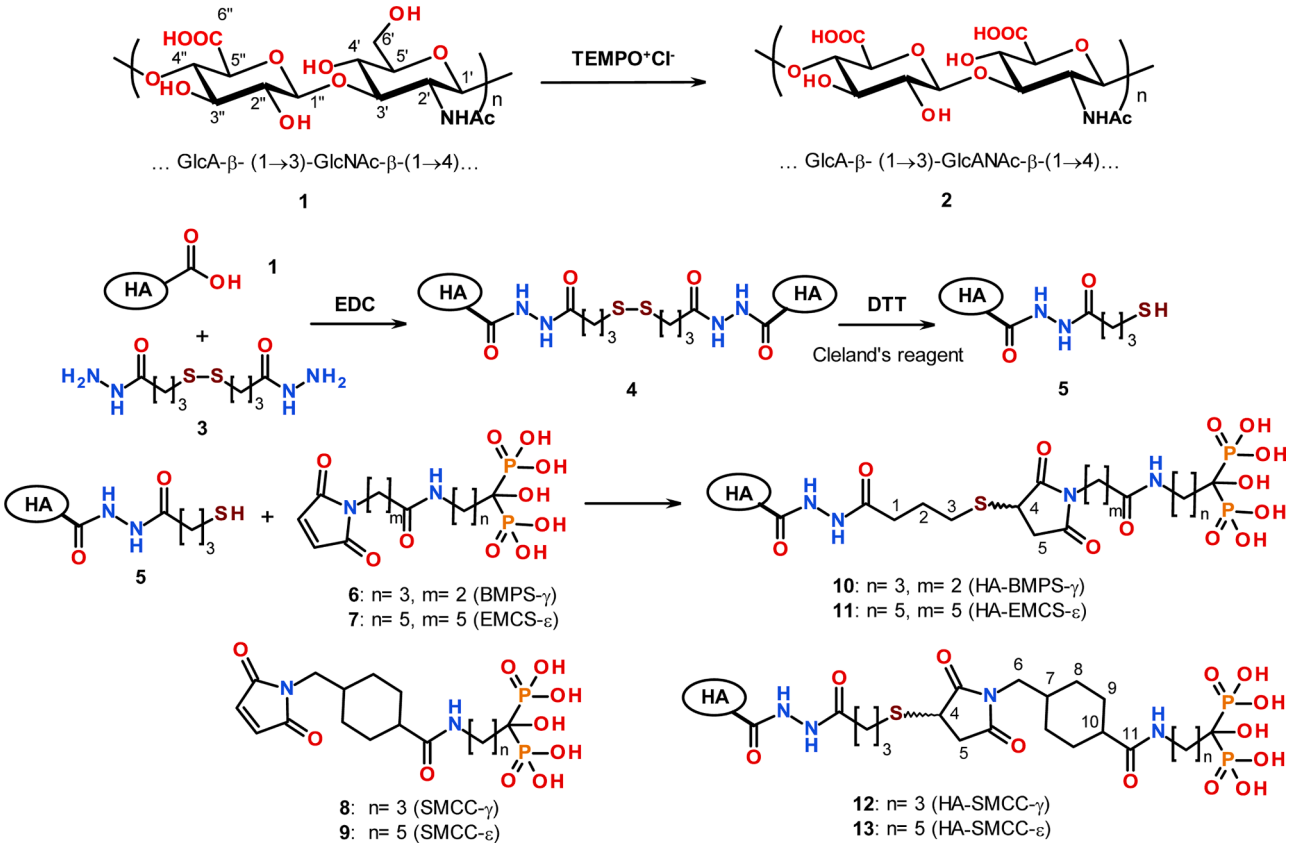

Scheme 1. Synthesis of compounds 2, 4–13.

Samples were prepared in a standard ampoule with a diameter of 5 mm. The chemical shifts of hydrogen atoms are given in the scale δ (ppm) relative to tetramethylsilane (TMS). One and two-dimensional NMR spectra (COSY ^1H–^1H, NOESY) were recorded using standard Bruker pulse sequences. IR spectra (thin films) were obtained with the use of a Bruker Vertex 70v spectrometer.

General procedure for the synthesis of conjugates of hyaluronic acid with amino acid bisphosphonates. To a solution of 20 mg of HA SH-derivative (5) in 4 ml of bidistilled water (0.05 mM, [C] = 0.01 mM/ml) with pH = 7 (pH was adjusted by adding 0.1 M NaOH solution), a previously prepared solution of maleimide derivative of aminobisphosphonate (6–9) (0.025 mM dissolved in 1 ml of bidistilled water) was added portionwise. The reaction mixture was stirred for 1–2 h at 36–38 °C, then it was transferred to a dialysis tape and dialyzed against a solution of bidistilled water (1 L containing 100 mM NaCl) within 1 day, followed by dialysis against distilled water for 2 days. Then the solvent was evaporated under reduced pressure. Compounds 10–13 were obtained in quantitative yield as a colorless film. IR (ν, cm^{-1}): 3400 (OH), 1377, 1142 (P=O), 2400 (CH_2).

HA-BMPS-γ (10) (SD = 25.5%). ^1H NMR (500.17 MHz, D_2O): 1.64–1.78 (m, 2H, C^9H_2), 1.79–1.89 (m, 2H, $C^{10}H_2$), 1.87–1.98 (m, 2H, C^2H_2), 1.93 (s, 3H, CO-CH_3, HA), 2.36–2.44 (m, 2H, C^7H_2), 2.39–2.48 (m, 2H, C^1H_2), 2.59–2.73 (m, 1H, C^5H_2), 2.65–2.78 (m, 2H, C^3H_2), 3.04–3.13 (m, 2H, C^8H_2), 3.17–3.31 (m, 1H, C^5H_2), 3.22–3.34 (m, 1H, $C^{2''}H$), 3.36–3.44 (m, 2H, C^6H_2), 3.33–3.53 (m, 2H, $C^{4'}H_2$, $C^{5'}H$), 3.61–3.74 (m, 4H, $C^{3'}H$, $C^{6'}H_2$, $C^{3''}H$, $C^{5''}H$), 3.74–3.82 (m, 2H, $C^{2'}H$, $C^{4''}H$), 3.82–3.92 (m, 1H, $C^{6'}H_2$), 3.90–4.02 (m, 1H, C^4H), 4.41–4.55 (m, 2H, $C^{1'}H$, $C^{1''}H$). ^{31}P NMR (202.48 MHz, D_2O): 17.78 ppm.

HA-EMCS-ε (11) (SD = 16.0%). ^1H NMR (500.17 MHz, D_2O): 1.14–1.28 (m, 2H, C^8H_2), 1.42–1.58 (m, 8H, C^7H_2, C^9H_2, $C^{12}H_2$, $C^{14}H_2$), 1.86–1.97 (m, 2H, C^2H_2), 1.94 (s, 3H, CO-CH_3, HA), 2.14 (t, $^3J = 7.2$ Hz, 2H, $C^{10}H_2$), 2.17–2.27 (m, 2H, $C^{15}H_2$), 2.21–2.31 (m, 2H, $C^{13}H_2$), 2.36–2.48 (m, 2H, C^1H_2), 2.59–2.73 (m, 1H, C^5H_2), 2.68–2.79 (m, 2H, C^3H_2), 3.06–3.15 (m, 2H, $C^{11}H_2$), 3.16–3.30 (m, 1H, C^5H_2), 3.20–3.33 (m, 1H, $C^{2''}H$), 3.38–3.49 (m, 2H, C^6H_2), 3.37–3.53 (m, 2H, $C^{4'}H$, $C^{5'}H$), 3.59–3.72 (m, 4H, $C^{3'}H$, $C^{6'}H_2$, $C^{3''}H$, $C^{5''}H$), 3.72–3.87 (m, 3H, $C^{2'}H$, $C^{6'}H_2$, $C^{4''}H$), 3.91–3.99 (m, 1H, C^4H), 4.31–4.57 (m, 2H, $C^{1'}H$, $C^{1''}H$). ^{31}P NMR (202 MHz, D_2O): 18.36 ppm.

HA-SMCC-γ (12) (SD = 20.6%). ^1H NMR (500.17 MHz, D_2O): 0.87–1.03 (m, 2H, C^8H_2), 1.21–1.28 (m, 2H, C^9H_2), 1.52–1.64 (m, 2H, C^7H_2), 1.60–1.69 (m, 2H, C^8H_2), 1.68–1.89 (m, 4H, $C^{12}H_2$, $C^{13}H_2$), 1.89–1.97 (m, 2H, C^2H_2), 1.94 (s, 3H, CO-CH_3, HA), 2.06–2.16 (m, 2H, $C^{10}H_2$), 2.41–2.47 (m, 2H, C^1H_2), 2.64–2.73 (m, 1H, C^5H_2), 2.68–2.74 (m, 2H, C^3H_2), 3.08–3.17 (m, 2H, $C^{11}H_2$), 3.20–3.30 (m, 1H, C^5H_2), 3.21–3.34 (m, 1H, $C^{2''}H$), 3.28–3.32 (m, 2H, C^6H_2), 3.35–3.54 (m, 2H, $C^{4'}H$, $C^{5'}H$), 3.58–3.72 (m, 4H, $C^{3'}H$, $C^{6'}H_2$, $C^{3''}H$, $C^{5''}H$), 3.73–4.00 (m, 3H, $C^{2'}H$, $C^{6'}H_2$, $C^{4''}H$), 3.94–4.00 (m, 1H, C^4H), 4.32–4.54 (m, 2H, $C^{1'}H$, $C^{1''}H$). ^{31}P NMR (202 MHz, D_2O): 18.36 ppm.

HA-SMCC-ε (13) (SD = 28.2%). ^{1}H NMR (500.17 MHz, D_2O): 0.88–1.00 (m, 2H, $C^{8}H_2$), 1.19–1.29 (m, 2H, $C^{13}H_2$), 1.39–1.50 (m, 4H, $C^{12}H_2$, $C^{14}H_2$,), 1.51–1.65 (m, 1H, $C^{7}H$), 1.60–1.70 (m, 2H, $C^{8}H_2$), 1.71–1.80 (m, 2H, $C^{9}H_2$), 1.82–1.89 (m, 2H, $C^{15}H_2$), 1.88–1.97 (m, 2H, $C^{2}H_2$), 1.94 (s, 3H, CO-CH_3, HA), 2.06–2.16 (m, 1H, $C^{10}H$), 2.39–2.48 (m, 2H, $C^{1}H_2$), 2.63–2.74 (m, 1H, $C^{5}H_2$), 2.66–2.79 (m, 2H, $C^{3}H_2$), 3.06–3.13 (m, 2H, $C^{11}H_2$), 3.19–3.29 (m, 1H, $C^{5}H_2$), 3.20–3.34 (m, 1H, $C^{2''}H$), 3.27–3.33 (m, 2H, $C^{6}H_2$), 3.34–3.54 (m, 2H, $C^{4'}H$, $C^{5'}H$), 3.58–3.73 (m, 4H, $C^{3'}H$, $C^{6'}H$, $C^{3''}H$, $C^{5''}H$), 3.73–3.88 (m, 3H, $C^{2'}H$, $C^{6'}H$, $C^{4''}H$), 3.92–4.01 (m, 1H, $C^{4}H$), 4.35–4.52 (m, 2H, $C^{1'}H$, $C^{1''}H$). ^{31}P NMR (202 MHz, D_2O): 18.36 ppm.

2.3. Surface characterization

The coating morphology was studied using Zeiss Gemini-300 scanning electron microscope (SEM). Average pore size and porosity (percentage of surface area occupied by pores) were determined from the SEM images using ImageJ software in accordance with ASTM E112-10. The coating thickness was measured with an eddy current thickness gage Defelsko Positector 6000. An optical Taylor Hobson Talysurf CCI profilometer was used to study the surface topography and surface roughness Ra, Rz. The adhesion strength test was carried out on a Revetest instrument (CSM instruments, Switzerland) using a diamond indenter with a radius of curvature of 200 μm.

XPS spectra were obtained using a JEOL JPS 9010MX spectrometer equipped with an (Mg K_α) X-ray source. The pressure in the analytical chamber during the spectral acquisition was less than 7×10^{-8} Pa. The survey spectra were collected from 0 to 1000 eV with a pass energy of 50 eV, and high-resolution spectra were collected for each detected element of interest (C, N, O, P, S, and Ti) with a pass energy of 10 eV. The JEOL SpecSurf Program V. 1.9.2 was used to identify the characteristic peaks, calculate the elemental compositions, and fit the peaks of the high-resolution spectra.

The contact angle (θ) of PEO treated Ti samples was measured by the sessile drop method with the Easy DROP instrument (DSA100, KRUSS, Germany) using distilled water as the contacting solvent. The drop image was captured by a video camera and an image analysis system was used to calculate the contact angle based on the average of left and right angles of each drop (Fig. S7, SI). Measurements were made for the left and right droplet angles on the sample, and the average contact angle was reported for all samples. The drop volume was equal to 9 μL; the experiment was carried out in 5 repetitions.

2.4. In vitro tests

Human embryonic lung fibroblasts (FLECH-104) and human adipose tissue mesenchymal stem cells (MSC) were purchased from BIOLOT (Russia), human osteosarcoma cells (MG-63) were obtained from the Russian collection of cell cultures of the Institute of Cytology RAS (Russia). FLECH-104 and MG-63 cells were cultured in a complete DMEM medium (Sigma) containing 10% fetal bovine serum (FBS) (BioWest), MSC in DMEM with 1 g/L glucose (Sigma) with 20% FBS in 25 cm^2 culture flasks (SPL Life Sciences) in a humidified atmosphere with 5% CO_2. The culture medium was changed twice a week. After reaching a monolayer, the cells were detached using 0.25% trypsin solution (PANECO) and counted using a TC20 (BioRad) automatic cell counter.

To assess the cytotoxicity of compounds 10–13, the MTT test was used, which assesses the metabolic activity of cells in proportion to their number. 5×10^3 MSC cells were plated into the wells of a 96-well culture plate, and upon reaching a monolayer, solutions of organic derivatives (0.1 mg/ml) were added to the complete medium in a ratio of 4:1, 6 holes of each type were used. MSCs were incubated with organic derivatives for 7 days under standard conditions (37 °C, 5 vol.% CO_2). The controls were cells in a complete culture medium. The medium was replaced with MTT solution 0.5 mg/ml for 2 h, and then with dimethyl sulfoxide to dissolve the formed formazan crystals. Absorbance was measured using a plate reader (Spark10M, Tecan) at 530 nm with a reference wavelength of 620 nm.

For the analysis of cell metabolic activity, we used a modification of the MTT test - EZ4U (Biomedica). The Ti samples coated with PEO were ultrasonically cleaned for 10 min in 95% ethanol, and then were rinsed with deionized water, air dried, and autoclaved at 134 °C. This temperature does not affect the PEO coating. PEO coated Ti samples were placed in a Petri dish with solutions of organic derivatives (1 mg/ml), which were pre-sterilized by filtration through a CA 0.22 μm filter. After 1 h, the samples were dried in the air in a laminar flow hood. Then all samples were placed in a 48-well culture plate. A suspension of MG-63, FLECH-104 or MSC cells were placed for 7 days in each well of a sample plate (0.4 ml, containing 6–10 $\times$ 10^3 cells) and were incubated under standard conditions. The cells in the wells with Ti-PEO samples were processed as controls. The well of the culture plate itself (polystyrene) was used to measure the background. Three samples of each type were transferred after incubation to another 48-well plate with 0.4 ml of fresh medium. Then 40 μl of activated EZ4U solution was added to each well and incubated at 37 °C, 5 vol.% CO_2 for 3.5 h. The optical absorption of the solution was analyzed at 450 nm with a reference wavelength of 620 nm. The relative percentage of EZ4U metabolization, normalized for the Ti-PEO group, was evaluated.

2.5. Statistical analysis

The mean value and the standard deviation for 6 (MTT) of 3 (EZ4U) measurements of the optical density were calculated with respect to the control. Data were analyzed using Kruskal-Wallis test with subsequent Dunn's multiple comparisons test (GraphPad Prism, v.6.01) at the significance level of $p < 0.05$.

2.6. Antimicrobial screening

Test cultures of S. aureus P 209, P. aeruginosa ATCC 27,853, and E. faecium Ef79OSAU were grown on Mueller-Hinton agar (HiMedia, India) at 37 °C for 18–24 h, then their suspensions were prepared in physiological saline with a density of 0.181; 0.184 and 0.228, respectively. The values of the optical density of the strains were determined empirically as a result of a series of experiments. Optical density was determined on a STAT FAX 2100 spectrophotometer at a wavelength of 492 nm.

100 μL of the bacterial suspension was added to the wells of a polypropylene plate with titanium samples. A separate row in the plate was occupied by suspensions of test strains without titanium samples, which was control of culture growth. Sterile Mueller-Hinton broth (HiMedia, India) was added to the other row as a sterility control and a blank for scanning wells. The plates were incubated at 37 °C. After 18–24 h, Ti samples were gently washed with PBS and then, to determine the number of adhered bacterial cells on the surface of titanium, they were stained with a 0.1% solution of gentian violet (Khimreaktivsnab, Russia). Further, the cells were destroyed with alcohol, and the optical density of the dye was measured, which comes out of destroyed cells [74]. The optical densities of the control and experimental samples were compared and the reliability of the difference using the methods of mathematical statistics was determined [75].

3. Results and discussion

3.1. Synthesis of hyaluronic acid bisphosphonates

As a basis for the introduction of aminobisphosphonates into a polysaccharide molecule, the corresponding SH-substituted HA (5) with a degree of functionalization of ~30% was obtained according to [71] (Scheme 1). For the synthesis of HA derivatives 10–13, N-maleimides of aminobisphosphonates of γ-butanoic and ε-caproic acids (6–9) were

preliminarily obtained via a procedure described in Ref. [65]. Further synthesis of bisphosphonates 10–13 was carried out via Michael addition through the reaction of the maleimide fragment of compounds 6–9 and the SH-group of the hyaluronic acid derivative 5. The result of the reaction depends on the pH of the media. It was found that in an acidic medium (pH 3.5) crosslinking of HA macromolecules occurs via SH-groups and the formation of disulfide bonds. In an alkaline medium (pH 9), the opening of the maleimide fragment of the linker was observed, which did not lead to the formation of the target conjugates. The carrying out of the conjugation reaction in a neutral medium (pH = 7) provided the addition of aminobisphosphonates (6–9) to the SH-group of the HA derivative (5) with a degree of substitution SD = 16.0–28.2%. Additional purification of the conjugates 10–13 in order to remove low molecular weight components was performed via the dialysis.

The structures of the new compounds 10–13 were confirmed by one- and two-dimensional NMR spectroscopy (Fig. 1, SI). The ^{1}H NMR spectra exhibited the signals corresponding to aminobisphosphonate, maleimide linker, and HA-S fragments. The addition of aminobisphosphonates to HA-SH was accompanied by the disappearance of the signal of the double bond protons of the maleimide fragment in the ^{1}H NMR spectrum at δ_H 6–7 ppm, as well as the shift of the characteristic signals of the H^{3} protons of the terminal thiol fragment of HA-SH from the δ_H 2.50–2.59 ppm to a lowfield region at δ_H 2.68–2.79 ppm. The COSY HH spectra showed cross-peaks between the signals of three protons with δ_H 2.59–2.73, 3.16–3.30, 3.91–3.99 ppm, belonging to the reduced maleimide fragment of the linker. The degree of substitution (SD) was determined from the ratio of the integral intensities of the signals of the anomeric HA protons in the region δ_H 4.35–4.52 ppm and methylene protons of aminobisphosphonate fragments at δ_H 1.0–1.7 ppm. The ^{31}P NMR spectra of 10–13 exhibited broadened signals at δ_P 17–19 ppm, characteristic to bisphosphonates.

3.2. Composite coating morphology and physicochemical properties

The morphological properties of PEO coatings on a coarse-grained and nanostructured substrate are shown in the SEM images in Fig. 2 and Table 2. The thickness of the PEO coating of the nano-Ti sample is slightly higher. The parameter of the average roughness Ra is practically the same for both samples, whereas the parameter Rz, characterizing the height of the maximum protrusions and valleys, is higher for the nano-Ti sample, which follows from Fig. 3.

The adhesion strength of the PEO coating to the nanostructured substrate is higher than to the CG substrate, as follows from the evaluation of a value of critical load (Table 2).

The porosity of PEO coatings on different substrates is the same; however, the average pore size distribution varies significantly (Fig. 4). In the case of nano-titanium substrate, the proportion of small pores with a size of 0.5–0.75 μm is greater than that of CG-Ti.

The formation of a combined coating on the surface of PEO-modified

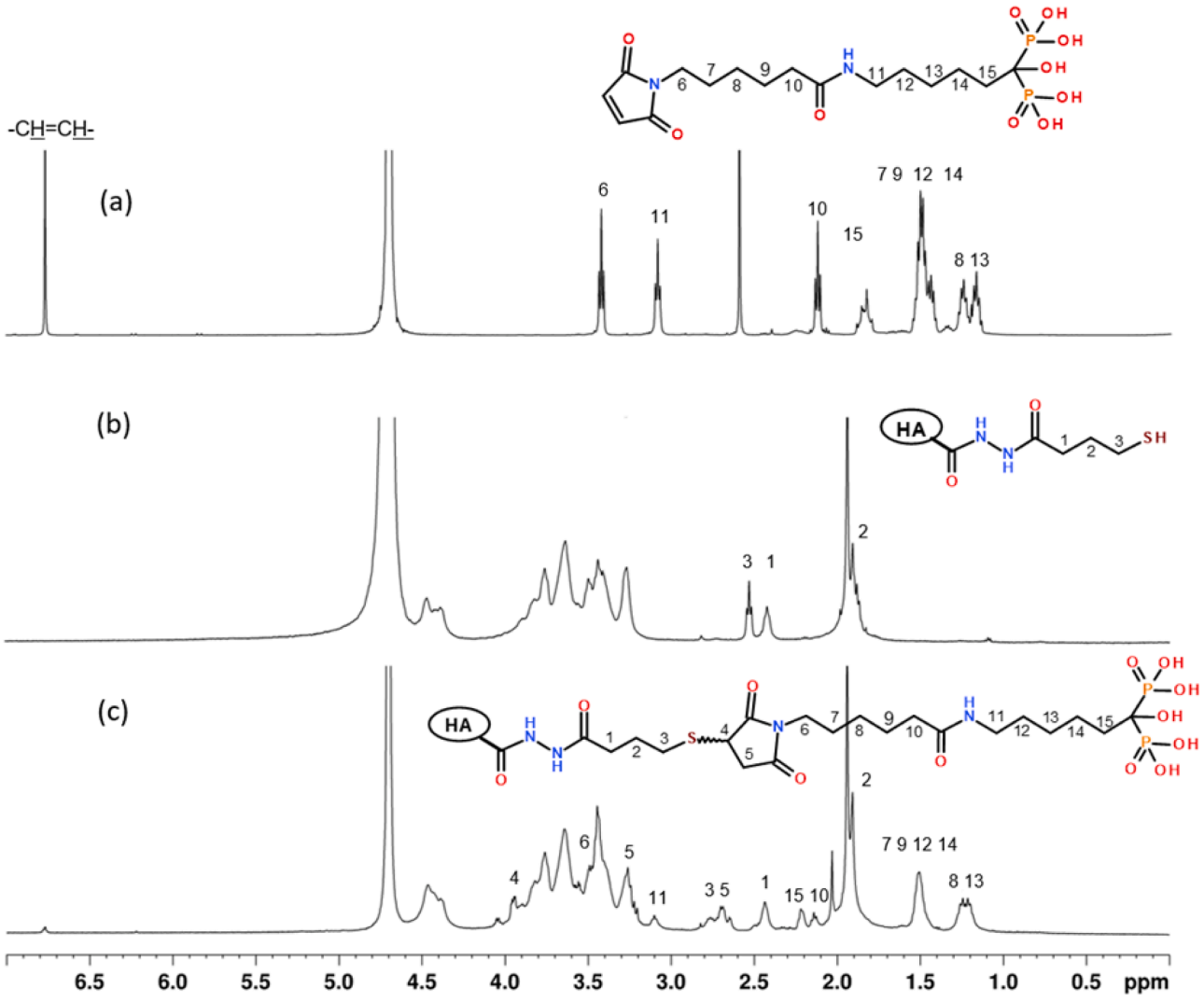

Fig. 1. H^{1} NMR spectra of compounds 5, 7, 11 in D_2O: (a) maleimidobisphosphonate EMCS-ε (7); (b) HA-SH (5) (SD = 30%); (c) the conjugate HA-EMCS-ε (11).

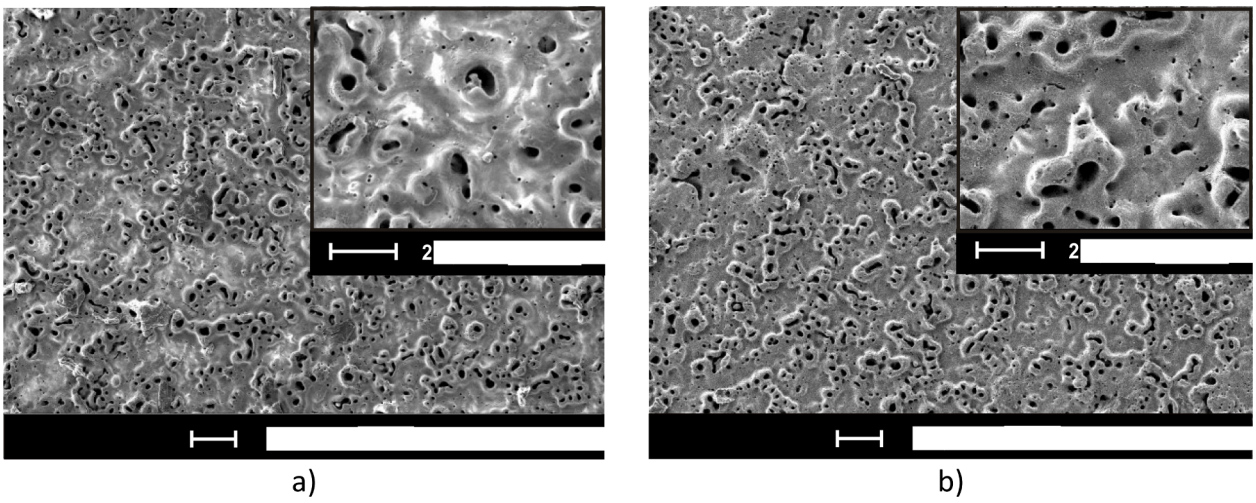

Fig. 2. SEM images of the top view of the PEO coatings CG-Ti (a), nano-Ti (b).

Table 2
Morphological properties of PEO coatings on coarse-grained and nanostructured substrates.

Sample	h (μm)	Rz (μm)	Ra (μm)	Porosity (%)	Average poresize (μm)	Criticalload, N
CG-Ti + PEO	18.9 ± 1.1	15.6 ± 0.54	2.6 ± 0.13	7.6 ± 1.4	1.44±0.17	4.9 ± 0.6
Nano-Ti + PEO	21.6 ± 1.3	17.3 ± 2.54	2.5 ± 0.05	7.6 ± 1.5	0.61±0.11	5.6 ± 0.7

titanium was carried out by applying organic layers due to.

The compounds 10–13 were introduced into the PEO coating via physicochemical adsorption from solutions with a concentration of 1 mg/ml. The presence of organic coating in the pores of the PEO sublayer was confirmed by X-ray photoelectron spectroscopy (XPS) (Table 3). Thus, the XPS spectra exhibited the peaks of Ti2p, Ti3s, O1s, C1s, P2p, N1s. XPS analysis showed the changes in the chemical composition of the surface of Ti-PEO after the coating with organic molecules. The greatest differences were observed in the spectra of Ti2p, C1s, O1s, and P2p. After the addition of the organic component, the relative intensity of the Ti2p line decreased and the intensities of C1s, O1s, and P2p increased, which resulted in a decrease in the ratio of Ti2p/C1s, Ti2p/O1s, and Ti2p/P2p.

To assess the effect of the organic coating on the hydrophilicity of the PEO-modified titanium surface, the contact angles were determined for the samples CG-Ti-PEO and nano-Ti-PEO in the absence and presence of a HA derivative 11 (Table 4).

As follows from Table 4, the surfaces of the initial Ti-PEO samples are hydrophilic. The appearance of organic molecules on the PEO-modified titanium leads to a decrease in the contact angle, which indicates an increase in the hydrophilicity of the surface.

3.3. In vitro study of the biological activity of coatings (cytotoxicity, viability, antimicrobial properties)

The *in vitro* toxicity of the obtained compounds was assessed using the MTT test (MSCs), as well as the degree of metabolic activity of various types of cells (osteoblast-like cells, fibroblasts, and mesenchymal stem cells) on the surface of CG-Ti-PEO and nano-Ti-PEO. The MTT test showed that HA and all HA derivatives are not only non-toxic but also promote cell growth. The highest growth-stimulating potential was found for the HA-EMCS-ε derivative (11) ($p < 0.0001$) (Fig. 5) that more than doubles cell viability. Such effect is unknown for HA phosphonates.

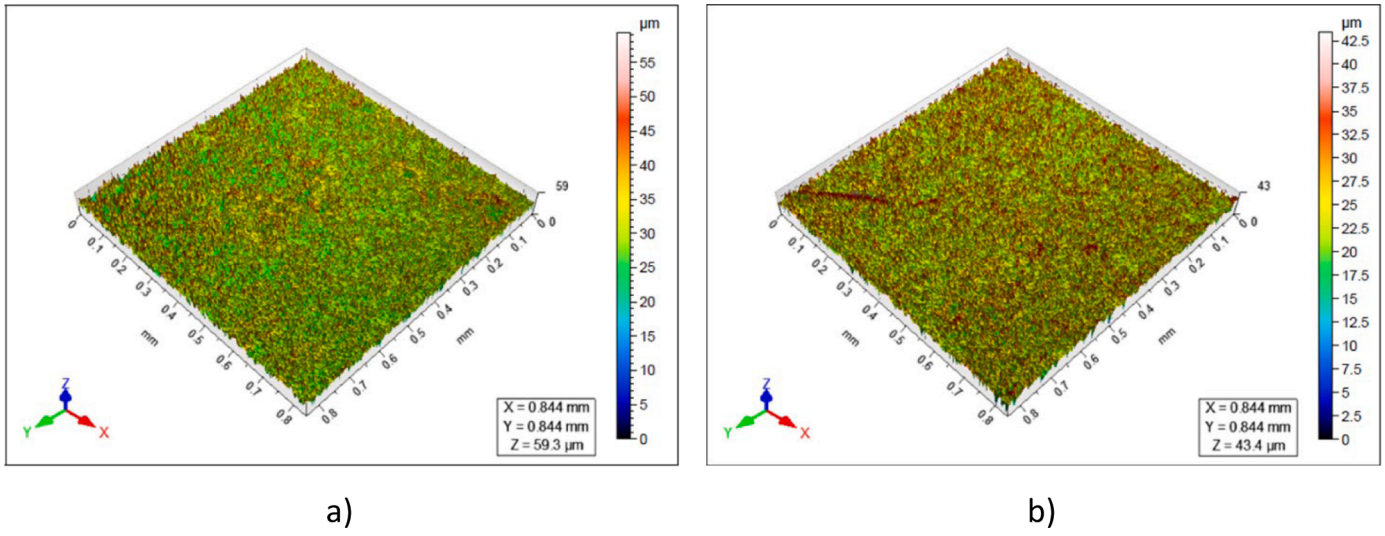

Fig. 3. Surface roughness of PEO coatings on CG-Ti (a) and nano-Ti (b) substrates.

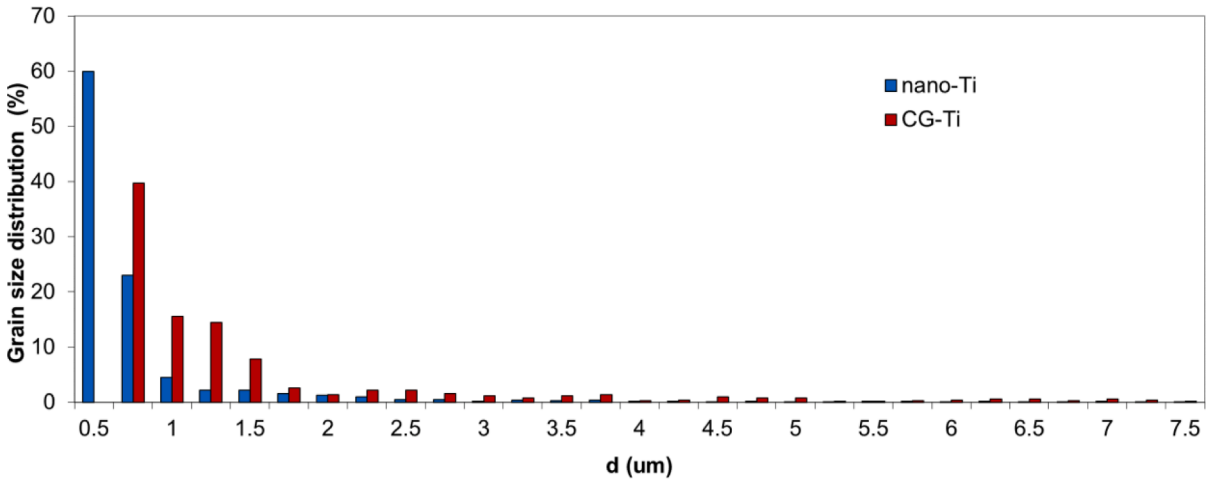

Fig. 4. Pore size distribution for CG-Ti-PEO and nano-Ti-PEO.

Table 3
Atomic composition and atomic ratio derived from XPS high-resolution spectra for the Ti-PEO samples with and without organic coating.

Sample		XPS Atomic composition (%)					Atomic ratio		
Type of organic coating	Substrate	N1s	P2p	C1s	O1s	Ti2p	Ti2p/C1s	Ti2p/O1s	Ti2p/P2p
	CG-Ti-PEO	1.73	3.44	13.43	69.32	12.08	0.90	0.17	3.51
	nano-Ti-PEO	0.97	2.97	11.34	73.55	11.17	0.99	0.15	3.76
HA (1)	CG-Ti-PEO	2.19	2.26	21.75	66.12	7.69	0.35	0.11	3.40
	nano-Ti-PEO	1.98	2.17	17.12	69.84	8.89	0.52	0.13	4.10
Carboxy-HA (2)	CG-Ti-PEO	0.94	2.97	18.83	69.02	8.24	0.44	0.12	2.77
	nano-Ti-PEO	1.19	3.54	16.28	67.06	11.93	0.73	0.18	3.37
HA-BMPS-γ (10)	CG-Ti-PEO	1.95	1.42	21.82	72.03	2.79	0.13	0.04	1.97
	nano-Ti-PEO	2.85	2.86	16.30	67.27	10.73	0.66	0.16	3.75
HA-EMCS-ε (11)	CG-Ti-PEO	2.40	2.00	30.02	60.16	5.41	0.18	0.09	2.71
	nano-Ti-PEO	1.71	2.59	21.42	65.72	8.55	0.40	0.13	3.30
HA-SMCC-γ (12)	CG-Ti-PEO	2.48	2.28	21.33	67.98	5.93	0.28	0.09	2.60
	nano-Ti-PEO	2.47	2.58	19.34	69.64	5.99	0.31	0.09	2.32
HA-SMCC- ε (13)	CG-Ti-PEO	1.64	2.13	13.17	76.89	6.17	0.47	0.08	2.90
	nano-Ti-PEO	1.78	1.69	14.42	76.44	5.67	0.39	0.07	3.36

Table 4
Contact angles θ for the Ti-PEO samples with and without organic coating HA-EMCS-ε (11).

Sample	Time, min		
	0	5	15
CG-Ti-PEO	67	53	37
nano-Ti-PEO	68	50	36
CG-Ti-PEO-HA-EMCS-ε (11)	60	42	27
nano-Ti-PEO-HA-EMCS-ε (11)	51	34	24

However, it is well known that hyaluronan influences cell adhesion, proliferation, differentiation, and migration via interaction with specific cellular receptors [30,32]. Moreover, hyaluronic acid can directly affect cell metabolic activity via mitochondria and increase the growth rate of stem cells, contribute to the extension of their lifespan with a reduction of cellular senescence, and prolong their differentiation potential [32]. Thereby, the mechanism of the influence of HA-EMCS-ε on cell viability requires an additional study.

As a result of the EZ4U metabolic test, it was shown that the introduction of phosphorylated HA and carboxy-HA into PEO-sublayer led to a decrease in the degree of viability of osteoblast-like MG-63 cells (at the level of 30–60%) and fibroblasts (at the level of 20–40%) after 7 days compared to the control Ti-PEO-surfaces (Fig. 6a,b). Moreover, a dependence of the degree of both MG-63 and MSC viability on the structure of the organic coating was observed. The least statistically

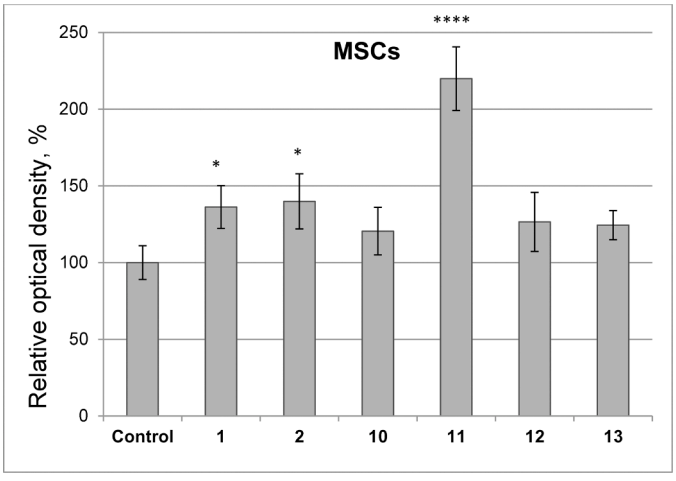

Fig. 5. Cytotoxicity of compounds 1, 2, 10–13 in the MTT test. Asterisks show significant differences with control ($p < 0.05$).

significant metabolic activity was found when using CG- and nano-Ti-PEO in combination with HA-SMCC-γ (12) ($p = 0.004$ and $p = 0.014$, respectively). The same molecule (12) provided a decrease in the metabolic activity of mesenchymal stem cells on Ti-PEO up to 55%, however, the differences were statistically significant only for the CG-Ti-

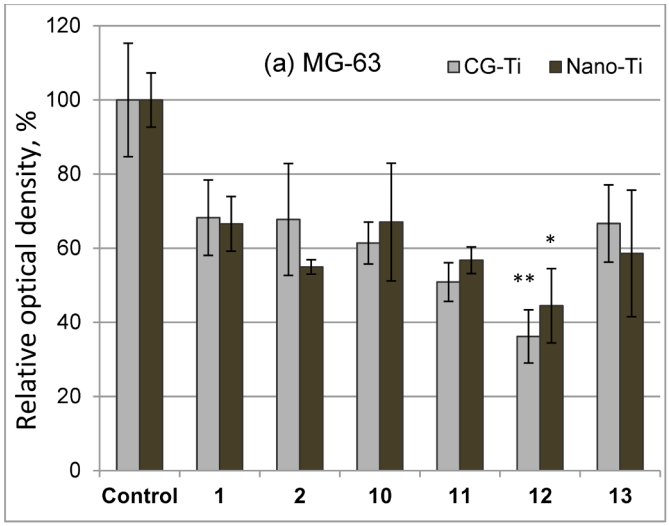

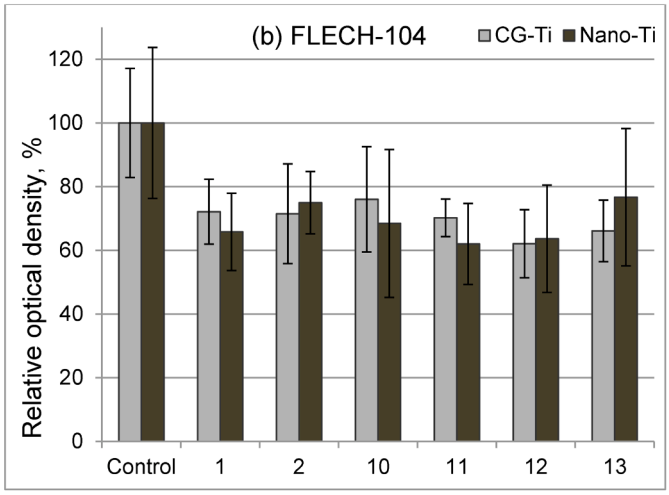

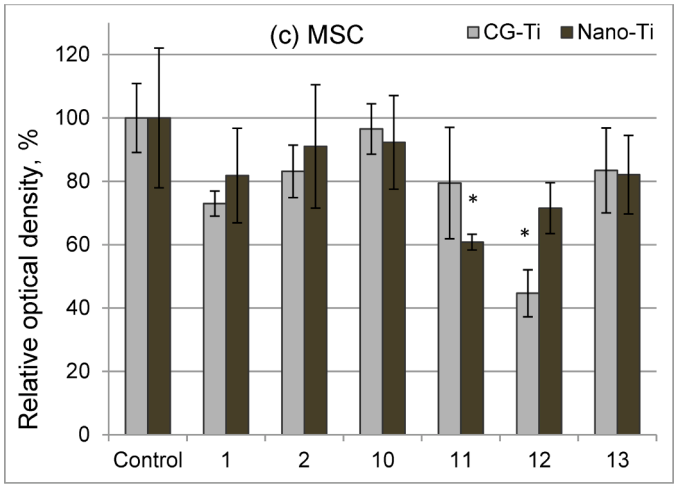

Fig. 6. Cell growth within 7 days by using an EZ4U *in vitro* assay for MG-63 osteoblast (a), FLECH-104 fibroblast (b) cell lines, and adipose-derived MSC cells (c) cultivated on Ti-PEO coated with compounds 1, 2, 10–13. Asterisks show significant differences with control Ti-PEO samples ($p < 0.05$).

PEO surface ($p = 0.023$). In addition, the HA-EMCS-ε (11) coating on nano-Ti also significantly reduced the viability of MSC cells ($p = 0.034$) (Fig. 6), while showing the ability to stimulate their growth in solution (Fig. 5). The effect of the organic molecule structure on the cell behavior can be caused by their orientation on the PEO surface during adsorption, which requires further studies. Thus, HA phosphonates can be considered as a promising base for the development of antifouling coatings for PEO-modified Ti implants.

The results of studies of the antibacterial properties of organic coatings, presented in Table 5, showed that the best effect is achieved for the modified polysaccharide (compounds 2, 10–13). The decrease in the degree of adhesion of microorganisms depended both on the structure of the organic molecule and the type of metal substrate (CG-Ti-PEO or nano-Ti-PEO).

Thus, the coatings carboxy-HA (2), HA-BMPS-γ (10), and HA-SMCC-γ (12) reduced the adhesion of gram-negative rod-shaped aerobic microorganisms P. aeruginosa on CG-Ti-PEO by 54%−56%. For HA-BMPS-γ (10), HA-EMCS-ε (11) and HA-SMCC-ε (13) degree of reduction of the bacteria adhesion on nano-Ti-PEO was more pronounced and amounted to 82–84%.

The inhibitory ability of all variants of biologically active coatings on CG-Ti-PEO towards gram-positive microorganisms S. aureus was more than 40%. Among them, HA-SMCC-γ (10) and HA-EMCS-ε (11) most effectively prevented the adhesion of the staphylococci (by 60% and 64%, respectively). For nano-Ti-PEO, an antimicrobial effect of 45–64% was shown in the case of using the compounds HA-BMPS-γ (10), HA-EMCS-ε (11), and HA-SMCC-ε (13).

The adhesion of enterococci E. faecium was reduced on CG-Ti-PEO by using HA and all its derivatives, among which the most effective were carboxy-HA (2) and HA-SMCC-γ (12), which inhibitory effect was 57%. As in the case of P. aeruginosa, the least amount of adhered E. faecium microorganisms was observed on the nano-Ti-PEO surface modified with organic compounds. In this case, the decrease in E. faecium adhesion was 79%, 68%, and 60% for carboxy-HA (2), HA-BMPS-γ (10), and HA-SMCC-ε (13) coatings, respectively.

Thus, the results of *in vitro* studies have shown the ability of the combined inorganic PEO coating and hyaluronic acid derivatives to reduce the number of osteoblast-like cells, fibroblasts, and MSCs, as well as the adhesion of microorganisms on the surface. This effect is apparently due to the known ability of polysaccharides, in particular glycosaminoglycans, to form a hydrophilic hydration layer on the surface, which prevents the adsorption of proteins on the surface, thereby giving

Table 5
The results of evaluating the effect of organic coatings 1, 2, 10–13 on the adhesion of microorganisms on the surface of CG-Ti-PEO and nano-Ti-PEO (the values of optical density and the percentage of change in optical density relative to the control sample without organic coating are shown).

Sample	P. aeruginosa (ATCC 27,853)		S. aureus (P 209)		E. faecium (Ef79OSAU)	
	CG-Ti-PEO	nano-Ti-PEO	CG-Ti-PEO	nano-Ti-PEO	CG-Ti-PEO	nano-Ti-PEO
Control	6.6 ± 0.1	5.1 ± 0.0	6.5 ± 0.2	5.3 ± 0.2	5.6 ± 0.2	5.3 ± 0.1
HA (1)	6.8 ± 0.0 +3.0%	5.9 ± 0.1 +15.7%	3.0 ± 0.1 −53.8%	5.8 ± 0.0 +9.4%	4.2 ± 0.1 −25.0%	4.7 ± 0.1 −11.3%
Carboxy-HA (2)	4.6 ± 0.1 −56.1%	3.2 ± 0.0 −37.2%	3.6 ± 0.1 −44.6%	4.6 ± 0.0 −13.2%	2.4 ± 0.1 −57.1%	1.1 ± 0.0 −79.2%
HA-BMPS-γ (10)	2.9 ± 0.2 −56.1%	0.9 ± 0.0 −82.3%	3.8 ± 0.1 −41.5%	2.5 ± 0.0 −52.8%	4.5 ± 0.0 −19.6%	1.7 ± 0.1 −67.9%
HA-EMCS-ε (11)	4.7 ± 0.0 −28.7%	0.9 ± 0.2 −82.3%	2.3 ± 0.2 −64.6%	2.9 ± 0.0 −45.3%	3.3 ± 0.2 −41.1%	7.5 ± 0.0 +41.5%
HA-SMCC-γ (12)	3.0 ± 0.1 −54.5%	4.4 ± 0.2 −13.7%	2.6 ± 0.2 −60.0%	3.5 ± 0.0 −33.9%	2.4 ± 0.2 −57.1%	2.7 ± 0.1 −49.1%
HA-SMCC-ε (13)	4.9 ± 0.0 −25.7%	0.8 ± 0.1 −84.3%	3.8 ± 0.0 −41.5%	1.9 ± 0.1 −64.1%	3.7 ± 0.0 −33.9%	2.1 ± 0.1 −60.3%

it antifouling properties [20,22]. Apparently, the appearance of an additional carboxyl function or bisphosphonate groups in HA leads to better fixation of the biopolymer on the surface and the creation of a hydration layer that effectively prevents cell adhesion. Modeling of antifouling surface properties is important for implants, as this can reduce the body's inflammatory response, resulting from the adhesion of proteins and immune cells [76,77]. In the case of hyaluronic acid derivatives, a decrease in the inflammatory response is possible not only due to the formation of a hydrophilic layer, and also due to the biological properties of the polysaccharide itself; specifically, the ability of HA to interact with various receptors such as CD44 and TSG-6 makes it a key regulator of inflammation: it creates a pericellular coating, which not only protects cells from inflammatory mediators, but also acts as an immunosuppressive agent, preventing access to ligands and inhibiting phagocytosis by macrophages and monocytes [33,34]. An increase in the hydrophilicity of the surface is also important for reducing the adhesion of pathogenic microorganisms [78–81]. The ability of polysaccharides to reduce the adhesion of microorganisms on the titanium surface due to changes in hydrophilicity has been repeatedly noted in the literature [50,51,82]. The HA derivatives obtained in this work are characterized by the effect of increasing the hydrophilicity of the surface. Apparently, this factor, along with the composition and structure of HA derivatives, which determine their orientation on the surface, are responsible for the antifouling and antimicrobial effect.

The influence of surface morphology on biological properties is seen in the adhesion of microorganisms to CG and nanostructured titanium (Table 5). Even in control samples that do not contain organic molecules, there is a decrease in the degree of bacteria adhesion of all studied types on the PEO surface obtained on nano-Ti. With the addition of an organic component, this effect is greatly enhanced in many cases. For nanostructured titanium, the roughness (Rz) of the PEO coating increases, therefore, one would expect an increase in pathogen adhesion, according to [83], although it was subsequently noted that there is no clear relationship between surface roughness and bacterial adhesion [79,84]. In our case, for nano-Ti, along with an increase in the Rz parameter, an increase in the proportion of small pores with the average size of 0.61 μm occurs, which is consistent with the tendency for the appearance of antimicrobial properties in the nanostructured surface, obtained as a result of anodizing as well [80]. Moreover, bacterial cells are several times smaller than eukaryotes and comparable in proportions to the pore sizes of the PEO coating on titanium. This is probably why they turned out to be more sensitive to surface morphology than eukaryotic cells.

Thus, we can conclude that modeling the surface properties by changing the chemical composition and morphology is an effective tool for the control of biological activity (Fig. 7), which can be successfully used further to create a new generation of implants with improved characteristics.

4. Conclusion

Thus, based on a biocompatible polysaccharide matrix - hyaluronic acid, we have synthesized hybrid molecules with bisphosphonate anchors. Due to the presence of bisphosphonate groups in the molecules, compounds can be introduced into the pores of the PEO coating by the physicochemical adsorption from solutions. The study of biological activity showed, that the compounds are non-toxic, and their introduction into the PEO coating reduces the viability of fibroblasts, osteoblast-like cells, and MSCs on the surface. Moreover, a significant decrease in the adhesion of bacteria P. aeruginosa, S. aureus, E. faecium on the surface of PEO-modified titanium containing HA derivatives was found. It is shown that the use of nanostructured titanium leads to an increase in the content of small pores on the PEO-modified surface (average pore size 0.61 μm), which in combination with an organic coating gives the effect of reducing the adhesion of pathogens up to 84%. The obtained results could be used for the development of a strategy for the creation of hybrid

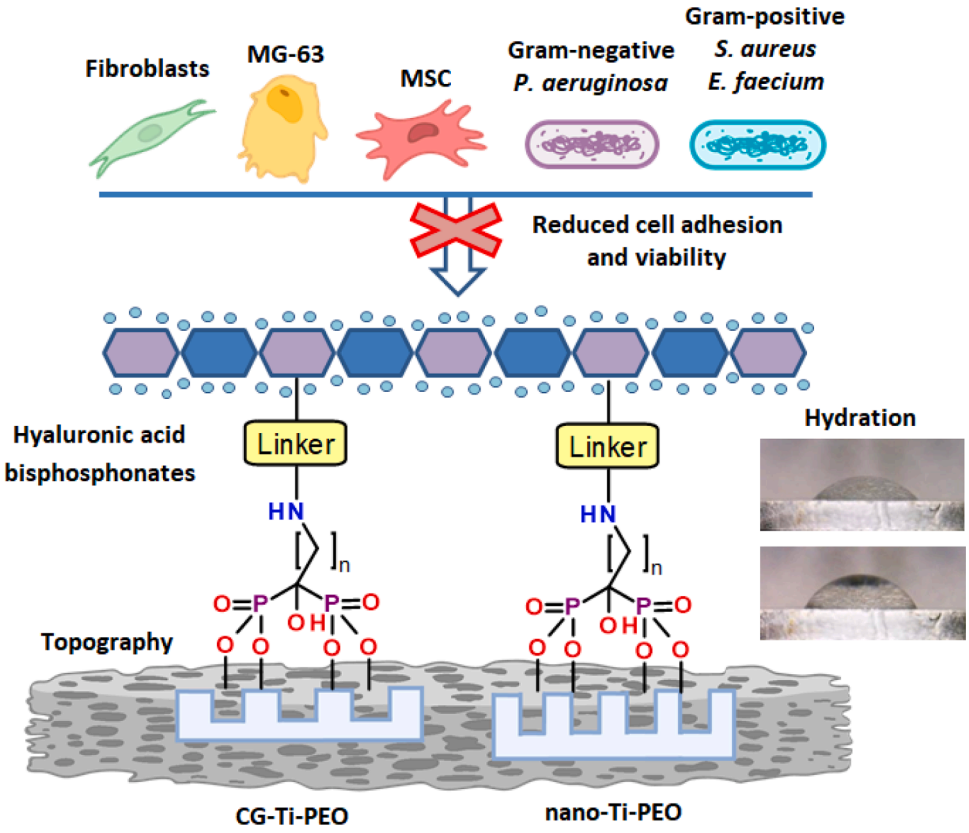

Fig. 7. Summary on protection effect of combined PEO-hyaluronic acid bisphosphonate coating.

organic-inorganic materials with improved biocompatibility based on plasma electrolytic oxidation and bioactive organic molecules.

Declaration of Competing Interest

The authors declare that they have no known competing financial interests or personal relationships that could have appeared to influence the work reported in this paper.

Acknowledgments

This work was supported by a grant from the Russian Science Foundation - DST (India) №. 19-49-02003. The structural studies of compounds 1-13 were carried out within the State Program of IPC RAS on unique equipment at the 'Agidel' Collective Usage Center (Ufa Federal Research Center, Russian Academy of Sciences, AAAA-A19-119022290012-3).

Supplementary materials

Supplementary material associated with this article can be found, in the online version, at doi:10.1016/j.surfin.2021.101678.

References

[1] C.N. Elias, J.H.C. Lima, R. Valiev, M.A. Meyers, Biomedical applications of titanium and its alloys, JOM 60 (3) (2008) 46–49.
[2] M. Geetha, A.K. Singh, R. Asokamani, A.K. Gogia, Ti based biomaterials, the ultimate choice for orthopaedic implants – a review, Prog. Mater. Sci. 54 (3) (2009) 397–425.
[3] Q. Chen, G.A. Thouas, Metallic implant biomaterials, Mater. Sci. Eng. R Rep. 87 (2015) 1–57.
[4] M. Rehman, A. Madni, T.J. Webster, The era of biofunctional biomaterials in orthopedics: what does the future hold? Expert Rev. Med. Devices 15 (3) (2018) 193–204.
[5] S. Wu, X. Liu, K.W.K. Yeung, C. Liu, X. Yang, Biomimetic porous scaffolds for bone tissue engineering, Mater. Sci. Eng. R. Rep. 80 (2014) 1–36.
[6] R.Z. Valiev, I. Sabirov, A.P. Zhilyaev, T.G. Langdon, Bulk nanostructured metals for innovative applications, JOM 64 (10) (2012) 1134–1142.
[7] A.V. Polyakov, L. Dluhoš, G.S. Dyakonov, G.I. Raab, R.Z. Valiev, Recent advances in processing and application of nanostructured titanium for dental implants, Adv. Eng. Mater. 17 (12) (2015) 1869–1875.
[8] B. An, Z. Li, X. Diao, H. Xin, Q. Zhang, X. Jia, Y. Wu, K. Li, Y. Guo, *In vitro* and *in vivo* studies of ultrafine-grain Ti as dental implant material processed by ECAP, Mater. Sci. Eng. C 67 (2016) 34–41.
[9] Y. Ito, N. Hoshi, T. Hayakawa, C. Ohkubo, H. Miura, K. Kimoto, Mechanical properties and biological responses of ultrafine-grained pure titanium fabricated by multi-directional forging, Mater. Sci. Eng. B 245 (2019) 30–36.
[10] K. Kalantari, B. Saleh, T.J. Webster, Biological applications of severely plastically deformed nano-grained medical devices: a review, Nanomaterials 11 (3) (2021) 748.
[11] R.A. Reiss, T.C. Lowe, J.A. Sena, O. Makhnin, M.C. Connick, P.E. Illescas, C. F. Davis, Bio-activating ultrafine grain titanium: RNA sequencing reveals enhanced mechano-activation of osteoconduction on nanostructured substrates, PLoS One 15 (9) (2020), e0237463.
[12] R.Z. Valiev, E.V. Parfenov, L.V. Parfenova, Developing nanostructured metals for manufacturing of medical implants with improved design and biofunctionality, Mater. Trans. 60 (7) (2019) 1356–1366.
[13] J. Vishnu, G. Manivasagam, Surface modification and biological approaches for tackling titanium wear-induced aseptic loosening, J. Bio Tribo Corros. 7 (1) (2021) 32.
[14] A. Nouri, C. Wen, C. Wen, 1 - Introduction to surface coating and modification for metallic biomaterials, Ed.. Surface Coating and Modification of Metallic Biomaterials, Woodhead Publishing, 2015, pp. 3–60.
[15] G.A. Momesso, A.M. de Souza Santos, J.M. Fonseca e Santos, N.C. da Cruz, R. Okamoto, V.A. Barão, R.S. Siroma, J.A. Shibli, L. Perez Faverani, Comparison between plasma electrolytic oxidation coating and sandblasted acid-etched surface treatment: histometric, tomographic, and expression levels of osteoclastogenic factors in osteoporotic rats, Materials 13 (7) (2020).
[16] A.L. Yerokhin, X. Nie, A. Leyland, A. Matthews, S.J. Dowey, Plasma electrolysis for surface engineering, Surf. Coat. Technol. 122 (2) (1999) 73–93.
[17] E.V. Parfenov, A. Yerokhin, R.R. Nevyantseva, M.V. Gorbatkov, C.J. Liang, A. Matthews, Towards smart electrolytic plasma technologies: an overview of methodological approaches to process modeling, Surf. Coat. Technol. 269 (2015) 2–22.
[18] M. Aliofkhazraei, D.D. Macdonald, E. Matykina, E.V. Parfenov, V.S. Egorkin, J. A. Curran, S.C. Troughton, S.L. Sinebryukhov, S.V. Gnedenkov, T. Lampke, F. Simchen, H.F. Nabavi, Review of plasma electrolytic oxidation of titanium substrates: mechanism, properties, applications and limitations, Appl. Surf. Sci. Adv. 5 (2021), 100121.
[19] T.O.B. Polo, W.P.P. Silva, G.A.C. Momesso, T.J. Lima-Neto, S. Barbosa, J. M. Cordeiro, J.S. Hassumi, N.C. da Cruz, R. Okamoto, V.A.R. Barão, L.P. Faverani, Plasma electrolytic oxidation as a feasible surface treatment for biomedical applications: an *in vivo* study, Sci. Rep. 10 (1) (2020) 10000.
[20] S.R. Meyers, M.W. Grinstaff, Biocompatible and bioactive surface modifications for prolonged *in vivo* efficacy, Chem. Rev. 112 (3) (2012) 1615–1632.
[21] G.B. Zhang, E.D. Myers, G.G. Wallace, M. Brandt, F.P. Choong, Bioactive coatings for orthopaedic implants—recent trends in development of implant coatings, Int. J. Mol. Sci. 15 (7) (2014).
[22] E. Lih, S.H. Oh, Y.K. Joung, J.H. Lee, D.K. Han, Polymers for cell/tissue anti-adhesion, Prog. Polym. Sci. 44 (2015) 28–61.
[23] L.B. Rice, Federal funding for the study of antimicrobial resistance in nosocomial pathogens: no ESKAPE, J. Infect. Dis. 197 (8) (2008) 1079–1081.
[24] C.W. Hall, T.-.F. Mah, Molecular mechanisms of biofilm-based antibiotic resistance and tolerance in pathogenic bacteria, FEMS Microbiol. Rev. 41 (3) (2017) 276–301.
[25] D. Sharma, L. Misba, A.U. Khan, Antibiotics versus biofilm: an emerging battleground in microbial communities, Antimicrob. Resist. Infect. Control 8 (1) (2019) 76.
[26] M. El-Azizi, S. Rao, T. Kanchanapoom, N. Khardori, *In vitro* activity of vancomycin, quinupristin/dalfopristin, and linezolid against intact and disrupted biofilms of staphylococci, Ann. Clin. Microbiol. Antimicrob. 4 (1) (2005) 2.
[27] R. Elashnikov, P. Ulbrich, B. Vokatá, V.S. Pavlíčková, V. Švorčík, O. Lyutakov, S. Rimpelová, Physically switchable antimicrobial surfaces and coatings: general concept and recent achievements, Nanomaterials 11 (11) (2021) 3083.
[28] P.J. Geutjes, W.F. Daamen, P. Buma, W.F. Feitz, K.A. Faraj, T.H. van Kuppevelt, From Molecules to Matrix: Construction and Evaluation of Molecularly Defined Bioscaffolds, Springer US, Boston, MA, 2007, pp. 279–295.
[29] A. Köwitsch, G. Zhou, T. Groth, Medical application of glycosaminoglycans: a review, J. Tissue Eng. Regen. Med. 12 (1) (2018) e23–e41.
[30] V. Nicola, S. Juergen, S. Robert, S. Ladislav, Role, metabolism, chemical modifications and applications of hyaluronan, Curr. Med. Chem. 16 (14) (2009) 1718–1745.
[31] E.R. Bastow, S. Byers, S.B. Golub, C.E. Clarkin, A.A. Pitsillides, A.J. Fosang, Hyaluronan synthesis and degradation in cartilage and bone, Cell. Mol. Life Sci. 65 (3) (2008) 395–413.
[32] M.A. Solis, Y.-.H. Chen, T.Y. Wong, V.Z. Bittencourt, Y.-.C. Lin, L.L.H. Huang, Hyaluronan regulates cell behavior: a potential niche matrix for stem cells, Biochem. Res. Int. 2012 (2012), 346972.
[33] A.J. Day, C.A. de la Motte, Hyaluronan cross-linking: a protective mechanism in inflammation? Trends Immunol. 26 (12) (2005) 637–643.
[34] R. Stern, A.A. Asari, K.N. Sugahara, Hyaluronan fragments: an information-rich system, Eur. J. Cell Biol. 85 (8) (2006) 699–715.
[35] C.E. Schanté, G. Zuber, C. Herlin, T.F. Vandamme, Chemical modifications of hyaluronic acid for the synthesis of derivatives for a broad range of biomedical applications, Carbohydr. Polym. 85 (3) (2011) 469–489.
[36] I.Y. Ponedel'kina, E.S. Lukina, E.A. Khaibrakhmanova, E.V. Sal'nikova, V. N. Odinokov, Conjugates of hyaluronic and carboxy hyaluronic acids and their *in vitro* biodegradability upon the action of testicular hyaluronidase, Russ. Chem. Bull. 60 (4) (2011) 754.
[37] L.G. Harris, L.M. Patterson, C. Bacon, I.a. Gwynn, R.G. Richards, Assessment of the cytocompatibility of different coated titanium surfaces to fibroblasts and osteoblasts, J. Biomed. Mater. Res. Part A 73A (1) (2005) 12–20.
[38] M. Morra, C. Cassinelli, A. Carpi, R. Giardino, M. Fini, Effects of molecular weight and surface functionalization on surface composition and cell adhesion to hyaluronan coated titanium, Biomed. Pharmacother. 60 (8) (2006) 365–369.
[39] M. Morra, C. Cassinelli, G. Cascardo, M. Fini, G. Giavaresi, R. Giardino, Covalently-linked hyaluronan promotes bone formation around Ti implants in a rabbit model, J. Orthop. Res. 27 (5) (2009) 657–663.
[40] D.S. Hwang, J.H. Waite, M. Tirrell, Promotion of osteoblast proliferation on complex coacervation-based hyaluronic acid – recombinant mussel adhesive protein coatings on titanium, Biomaterials 31 (6) (2010) 1080–1084.
[41] H.S. Seo, B.H. Kim, Y.M. Ko, Fabrication of anodized titanium with immobilization of hyaluronic acid to improve biological performance, Prog. Org. Coat. 69 (1) (2010) 38–44.
[42] H. Ao, Y. Xie, H. Tan, S. Yang, K. Li, X. Wu, X. Zheng, T. Tang, Fabrication and *in vitro* evaluation of stable collagen/hyaluronic acid biomimetic multilayer on titanium coatings, J. R. Soc. Interface 10 (84) (2013), 20130070.
[43] H. Ao, Y. Xie, A. Qin, H. Ji, S. Yang, L. Huang, X. Zheng, T. Tang, Immobilization of hyaluronic acid on plasma-sprayed porous titanium coatings for improving biological properties, J. Biomater. Sci. Polym. Ed. 25 (11) (2014) 1211–1224.
[44] H. Ao, C. Lin, B. Nie, S. Yang, Y. Xie, Y. Wan, X. Zheng, The synergistic effect of type I collagen and hyaluronic acid on the biological properties of Col/HA-multilayer-modified titanium coatings: an *in vitro* and *in vivo* study, RSC Adv. 7 (42) (2017) 25828–25837.
[45] Z. Yuan, S. Huang, S. Lan, H. Xiong, B. Tao, Y. Ding, Y. Liu, P. Liu, K. Cai, Surface engineering of titanium implants with enzyme-triggered antibacterial properties and enhanced osseointegration *in vivo*, J. Mater. Chem. B 6 (48) (2018) 8090–8104.
[46] H. Ao, S. Yang, B.e. Nie, Q. Fan, Q. Zhang, J. Zong, S. Guo, X. Zheng, T. Tang, Improved antibacterial properties of collagen I/hyaluronic acid/quaternized chitosan multilayer modified titanium coatings with both contact-killing and release-killing functions, J. Mater. Chem. B 7 (11) (2019) 1951–1961.

[47] S. Agarwal, B. Duffy, J. Curtin, S. Jaiswal, Effect of high- and low-molecular-weight hyaluronic-acid-functionalized-AZ31 Mg and Ti alloys on proliferation and differentiation of osteoblast cells, ACS Biomater. Sci. Eng. 4 (11) (2018) 3874–3884.
[48] J.H. Lee, Y.Z. Jin, Recombinant human bone morphogenetic protein-2 loaded porous β-tricalcium phosphate microsphere-hyaluronic acid composites promoted osseointegration around titanium implants, Int. J. Polym. Mater. Polym. Biomater. 68 (7) (2019) 368–374.
[49] Q. Wang, Y.-b. Hong, M.-d. Huang, Q.-m. Wang, W. Teng, Constructing self-adhesive and robust functional films on titanium resistant to mechanical damage during dental implanting, Mater. Sci. Eng. C 110 (2020), 110688.
[50] X. Hu, K.-.G. Neoh, Z. Shi, E.-.T. Kang, C. Poh, W. Wang, An *in vitro* assessment of titanium functionalized with polysaccharides conjugated with vascular endothelial growth factor for enhanced osseointegration and inhibition of bacterial adhesion, Biomaterials 31 (34) (2010) 8854–8863.
[51] P.H. Chua, K.G. Neoh, Z. Shi, E.T. Kang, Structural stability and bioapplicability assessment of hyaluronic acid–chitosan polyelectrolyte multilayers on titanium substrates, J. Biomed. Mater. Res. Part A 87A (4) (2008) 1061–1074.
[52] C. Queffélec, M. Petit, P. Janvier, D.A. Knight, B. Bujoli, Surface modification using phosphonic acids and esters, Chem. Rev. 112 (7) (2012) 3777–3807.
[53] J. Goura, V. Chandrasekhar, Molecular Metal Phosphonates, Chem. Rev. 115 (14) (2015) 6854–6965.
[54] B. Bujoli, C. Queffelec, Fine-tuning the functionality of inorganic surfaces using phosphonate chemistry. Tailored Organic-Inorganic Materials, 2015, pp. 299–318.
[55] E.S. Gawalt, M.J. Avaltroni, N. Koch, J. Schwartz, Self-assembly and bonding of alkanephosphonic acids on the native oxide surface of titanium, Langmuir 17 (19) (2001) 5736–5738.
[56] G. Lecollinet, N. Delorme, M. Edely, A. Gibaud, J.F. Bardeau, F. Hindré, F. Boury, D. Portet, Self-assembled monolayers of bisphosphonates: influence of side chain steric hindrance, Langmuir 25 (14) (2009) 7828–7835.
[57] N. Illy, M. Fache, R. Ménard, C. Negrell, S. Caillol, G. David, Phosphorylation of bio-based compounds: the state of the art, Polym. Chem. 6 (35) (2015) 6257–6291.
[58] O.P. Varghese, W. Sun, J. Hilborn, D.A. Ossipov, *In situ* cross-linkable high molecular weight hyaluronan–bisphosphonate conjugate for localized delivery and cell-specific targeting: a hydrogel linked prodrug approach, J. Am. Chem. Soc. 131 (25) (2009) 8781–8783.
[59] X. Yang, S. Akhtar, S. Rubino, K. Leifer, J. Hilborn, D. Ossipov, Direct ″click″ synthesis of hybrid bisphosphonate–hyaluronic acid hydrogel in aqueous solution for biomineralization, Chem. Mater. 24 (9) (2012) 1690–1697.
[60] G. Hulsart-Billström, P.K. Yuen, R. Marsell, J. Hilborn, S. Larsson, D. Ossipov, Bisphosphonate-linked hyaluronic acid hydrogel sequesters and enzymatically releases active bone morphogenetic protein-2 for induction of osteogenic differentiation, Biomacromolecules 14 (9) (2013) 3055–3063.
[61] D.A. Ossipov, Bisphosphonate-modified biomaterials for drug delivery and bone tissue engineering, Expert Opin. Drug Deliv. 12 (9) (2015) 1443–1458.
[62] I. Berts, D. Ossipov, G. Fragneto, A. Frisk, A.R. Rennie, Polymeric smart coating strategy for titanium implants, Adv. Eng. Mater. 16 (11) (2014) 1340–1350.
[63] L. Shi, Y. Zeng, Y. Zhao, B. Yang, D. Ossipov, C.-.W. Tai, J. Dai, C. Xu, Biocompatible injectable magnetic hydrogel formed by dynamic coordination network, ACS Appl. Mater. Interfaces 11 (49) (2019) 46233–46240.
[64] E.V. Parfenov, L.V. Parfenova, G.S. Dyakonov, K.V. Danilko, V.R. Mukaeva, R. G. Farrakhov, E.S. Lukina, R.Z. Valiev, Surface functionalization via PEO coating and RGD peptide for nanostructured titanium implants and their *in vitro* assessment, Surf. Coat. Technol. 357 (2019) 669–683.
[65] L.V. Parfenova, E.S. Lukina, Z.R. Galimshina, G.U. Gil'fanova, V.R. Mukaeva, R. G. Farrakhov, K.V. Danilko, G.S. Dyakonov, E.V. Parfenov, Biocompatible organic coatings based on bisphosphonic acid RGD-derivatives for PEO-modified titanium implants, Molecules 25 (1) (2020) 229.
[66] E. Parfenov, L. Parfenova, V. Mukaeva, R. Farrakhov, A. Stotskiy, A. Raab, K. Danilko, N. Rameshbabu, R. Valiev, Biofunctionalization of PEO coatings on titanium implants with inorganic and organic substances, Surf. Coat. Technol. 404 (2020), 126486.
[67] D.V. Gunderov, A.V. Polyakov, I.P. Semenova, G.I. Raab, A.A. Churakova, E. I. Gimaltdinova, I. Sabirov, J. Segurado, V.D. Sitdikov, I.V. Alexandrov, N. A. Enikeev, R.Z. Valiev, Evolution of microstructure, macrotexture and mechanical properties of commercially pure Ti during ECAP-conform processing and drawing, Mater. Sci. Eng. A 562 (2013) 128–136.
[68] G.S. Dyakonov, E. Zemtsova, S. Mironov, I.P. Semenova, R.Z. Valiev, S.L. Semiatin, An EBSD investigation of ultrafine-grain titanium for biomedical applications, Mater. Sci. Eng. A 648 (2015) 305–310.
[69] I.Y. Ponedel'kina, E.A. Khaibrakhmanova, T.V. Tyumkina, I.V. Romadova, V. N. Odinokov, Stoichiometric C6-oxidation of hyaluronic acid by oxoammonium salt TEMPO+Cl− in an aqueous alkaline medium, Carbohydr. Polym. 130 (2015) 69–76.
[70] K.P. Vercruysse, D.M. Marecak, J.F. Marecek, G.D. Prestwich, Synthesis and *in vitro* degradation of new polyvalent hydrazide cross-linked hydrogels of hyaluronic acid, Bioconjug. Chem. 8 (5) (1997) 686–694.
[71] X.Z. Shu, Y. Liu, Y. Luo, M.C. Roberts, G.D. Prestwich, Disulfide cross-linked hyaluronan hydrogels, Biomacromolecules 3 (6) (2002) 1304–1311.
[72] O. Nielsen, O. Buchardt, Facile synthesis of reagents containing a terminal maleimido ligand linked to an active ester, Synthesis 1991 (10) (1991) 819–821 (Mass).
[73] N.J. Ede, G.W. Tregear, J. Haralambidis, Routine preparation of thiol oligonucleotides: application to the synthesis of oligonucleotide-peptide hybrids, Bioconjug. Chem. 5 (4) (1994) 373–378.
[74] G. O'Toole, H.B. Kaplan, R. Kolter, Biofilm formation as microbial development, Annu. Rev. Microbiol. 54 (1) (2000) 49–79.
[75] G.F. Lakin, Biometriya, Vysshaya shkola, Moscow, 1990.
[76] D. Lee, K. Park, J. Seo, Recent advances in anti-inflammatory strategies for implantable biosensors and medical implants, Biochip J. 14 (1) (2020) 48–62.
[77] E. Mariani, G. Lisignoli, R.M. Borzì, L. Pulsatelli, Biomaterials: foreign bodies or tuners for the immune response? Int. J. Mol. Sci. 20 (3) (2019) 636.
[78] L. Zhao, P.K. Chu, Y. Zhang, Z. Wu, Antibacterial coatings on titanium implants, J. Biomed. Mater. Res. Part B Appl. Biomater. 91B (1) (2009) 470–480.
[79] A. Han, J.K.H. Tsoi, F.P. Rodrigues, J.G. Leprince, W.M. Palin, Bacterial adhesion mechanisms on dental implant surfaces and the influencing factors, Int. J. Adhes. Adhes. 69 (2016) 58–71.
[80] H. Chouirfa, H. Bouloussa, V. Migonney, C. Falentin-Daudré, Review of titanium surface modification techniques and coatings for antibacterial applications, Acta Biomater. 83 (2019) 37–54.
[81] A. Escobar, N. Muzzio, S.E. Moya, Antibacterial layer-by-layer coatings for medical implants, Pharmaceutics 13 (1) (2021) 16.
[82] H. Lv, Z. Chen, X. Yang, L. Cen, X. Zhang, P. Gao, Layer-by-layer self-assembly of minocycline-loaded chitosan/alginate multilayer on titanium substrates to inhibit biofilm formation, J. Dent. 42 (11) (2014) 1464–1472.
[83] M. Quirynen, C.M.L. Bollen, The influence of surface roughness and surface-free energy on supra- and subgingival plaque formation in man, J. Clin. Periodontol. 22 (1) (1995) 1–14.
[84] M. Katsikogianni, Y.F. Missirlis, Concise review of mechanisms of bacterial adhesion to biomaterials and of techniques used in estimating bacteria-material interactions, Eur. Cell Mater. 8 (2004) 37–57.